Physical Characteristics and Cell-Adhesive Properties of *In Vivo* Fabricated Hyaluronan/Bacterial Cellulose Nanocomposites

Ryo Takahama
Kyushu University
Honami Kato
Kyushu University
Go Takayama
Kyushu University
Kenji Tajima
Hokkaido University
Tetsuo Kondo (tekondo@agr.kyushu-u.ac.jp)
Kyushu University https://orcid.org/0000-0003-4366-2955

Research Article

Keywords: Hyaluronan/bacterial cellulose nanocomposite, Hyaluronan, Bacterial cellulose nanofibril, Nanocomposite, In vivo production

Posted Date: December 9th, 2021

DOI: https://doi.org/10.21203/rs.3.rs-1115449/v1

Version of Record: A version of this preprint was published at Cellulose on March 7th, 2022. See the published version at https://doi.org/10.1007/s10570-022-04480-2.

Abstract

This study attempts to clarify the basic material properties of *in-vivo*-fabricated hyaluronan (HA)/bacterial cellulose (BC) nanocomposites prepared previously. BC membranes (pellicles) generated by *Gluconacetobacter hansenii* (*G. hansenii*) are promising biomaterials owing to their outstanding biocompatible properties. Recently, specific demands for biomedical applications of BC have increased owing to its excellent mechanical properties. Although many techniques have been developed to improve the biofunctional properties of BC pellicles, such modifications remain limited owing to technical difficulties in the modulation of complex biosynthetic processes. Therefore, we previously developed an *in vivo* modification technique to produce nanocomposite pellicles composed of BC and HA (*in vivo* HA/BC), which are directly secreted from genetically engineered *G. hansenii*. In the present study, the HA extractability and content rate, physical characteristics, and cytocompatibility of *in vivo* HA/BC have been investigated in comparison to conventional *in situ* HA/BC and native BC pellicle. The results suggested that HA more strongly adsorbed to the solid BC surface of *in vivo* HA/BC than that of *in situ* HA/BC, which possibly affected the dynamic viscoelastic characteristics. Furthermore, *in vivo* HA/BC showed remarkably high human epidermal cell adhesion. These results indicate the great potential of *in vivo* modification to expand the usefulness of BC-based biomaterials.

Introduction

Bacterial cellulose (BC) synthesized by several bacterial species in the family *Acetobacteraceae* exhibits unique structural and physical characteristics, which are highly beneficial in various applications, particularly in biomedical science. *Gluconacetobacter hansenii* (*G. hansenii*, recently reclassified as *Komagataeibacter hansenii*) produces a gel-like BC membrane (pellicle) layer at the air–liquid interface of the culture medium, and contains a network structure of highly crystalline BC nanofibrils that results in entrapping of the culture media and bacterial cells. Unlike plants and other organisms, *G. hansenii* constructs this extracellular network substance from pure cellulose owing to the function of transmembrane cellulose-synthesizing protein complexes (Tajima and Yao 2021).

The excellent chemical purity of cellulose in BC pellicles also contributes to outstanding mechanical characteristics (Young's modulus in tensile deformation of 16–18 GPa in the form of dehydrated sheet; Yamanaka et al. 1989; M. Iguchi; et al. 2000), owing to efficient hydrogen bond engagements between BC nanofibrils (Yamanaka et al. 1989; Nishi et al. 1990). As BC pellicles can easily be refined and behave like a hydrogel comprising biologically inert cellulose and water entrained in nano- to microscale pores, they also exhibit excellent biocompatible properties (Helenius et al. 2006; Ludwicka et al. 2016) superior to those of ultrahigh-molecular-weight polyethylene (UHMWPE), which is a synthetic biocompatible material commonly used in orthopedic applications (*in vivo* in rats) (Grobelski et al. 2014). These fascinating characteristics of BC pellicles have motivated a large number of studies toward various applications (Klemm et al. 2018), particularly in the field of biomedical science (Ludwicka et al. 2016).

Although BC pellicles are a highly promising biomaterial, challenges remain regarding modification of their surface or bulk properties to meet specific biological and physical requirements, especially enhancing the affinity with cells seeded on them. Ludwicka et al. (2016) have classified the biomedical uses of BC pellicles into three types, as follows: Wound dressings, implants, and scaffolds for tissue engineering (and drug delivery systems derived from these applications). BC-based wound dressings and implant parts have already been commercialized in several countries, including Brazil, Germany, Poland, and USA. However, controlling the porosity (surface and bulk) and cell–substrate interactions are issues that should be resolved to allow BC applications in other implant parts and tissue engineering. The pore size (or nanofibril density) of BC pellicle surfaces is crucial for cell attachment and growth (Berti et al. 2013), but the typical pore size of the natural BC pellicle surface (several hundred nm scale) is too small for mammalian cell (at least 10 μm) ingrowth. Therefore, much effort has been made to control or expand the pores of BC pellicles to facilitate cells settling on the surface or inside the nanofibril network (Bäckdahl et al. 2008; Sämfors et al. 2019). Furthermore, porosity affects the mechanical characteristics, particularly stiffness (Hutmacher et al. 2014), which further modulates the cell behavior through mechanotransduction (Tsimbouri et al. 2014). Cell–substrate interactions are affected not only by such surface topography and physical characteristics, but also by the cell type and surface chemistry of the material (Tsimbouri et al. 2014). As pure BC pellicle surfaces are not superior substrates for the adherence, spreading, and proliferation of anchorage-dependent cells (Watanabe et al. 1993), many techniques have been developed to modify the surface chemical features of this material (Gorgieva 2020; Klemm et al. 2018). Therefore, expanding the biomedical use of BC pellicles to more advanced and specific applications, such as tissue engineering, where modification of the surface and bulk properties is of importance, remains challenging.

In previous reports, we developed an *in vivo* fabrication technique for the production of a polysaccharide nanocomposite of curdlan and BC (Fang et al. 2015), and hyaluronan (HA) and BC (Takahama et al. 2021), using genetically engineered *G. hansenii* with introduction of minimum and essential genes for these biosyntheses. Related to the present study, the engineered *G. hansenii* (hereafter referred to as Gh(HA)) successfully synthesized HA and, more importantly, extruded from one side of the bacterial cell surface. The secreted product was a nanofibril-like structure similar to that obtained by native BC biosynthesis. As HA within this structure is strongly adhered to the crystalline BC surface, *in-vivo*-synthesized HA/BC is expected to exhibit superior biological functions leading to the further applicability of BC-based materials in biomedical science.

In this study, the basic material characteristics of *in-vivo*-synthesized HA/BC, including HA content, biodegradation properties, nanofibril network structure, mechanical characteristics, and interaction with human cells, were compared with those of native BC and composites mechanically formed in the culture media (namely, in situ HA/BC).

Materials And Methods

Materials

D-Glucose was purchased from Sigma-Aldrich (MO, USA), and Bacto-yeast extract, peptone, and agar were purchased from Difco Laboratories Inc. (NJ, USA). Disodium hydrogen phosphate heptahydrate ($Na_2HPO_4{\cdot}7H_2O$) was purchased from Nacalai Tesque Inc. (Kyoto, Japan). Citric acid, ampicillin sodium, glycerol, and lysozyme were purchased from Wako Pure Chemical Industries, Ltd. (Osaka, Japan). Cellulase "ONOZUKA" R-10 was purchased from Yakult Pharmaceutical Industry Co., Ltd. (Tokyo, Japan). Sodium hyaluronate FCH-60 was purchased from Kikkoman Biochemifa Co. (Tokyo, Japan). All other chemicals were of reagent-grade quality or better. *Gluconacetobacter hansenii* (present name is *Komagataeibacter hansenii*) ATCC 23769 was purchased from the American Type Culture Collection.

Bacterial strains and transformation

All procedures were according to our previous report (Takahama et al. 2021). Briefly, plasmids were introduced into *Gluconacetobacter hansenii* ATCC23769 (Gh) by electroporation (Hall et al. 1992) to obtain Gh(HA), an HA-producing transformant, and Gh(pTI99), a negative control (Sunagawa et al. 2012; Fang et al. 2015) carrying a plasmid vector without genes for HA synthesis. Positive clones with a high cellulose-producing ability were selected. After incubation for 3 days, colonies on the HS–agar plates were transferred to liquid HS medium containing ampicillin sodium (Amp) and cellulase, and grown at 30 °C under continuous rotary shaking (125 rpm) for 22–24 h. This culture broth was also used as a seed culture for the following culture for nanocomposite production.

Nanocomposite production and purification

According to our previous report on nanocomposites production (Takahama et al. 2021), Gh transformants (Gh(HA) and Gh(pTI99)) were grown in two culture steps, namely, pre-culture and main culture. Briefly, the seed culture was inoculated to HS medium supplemented with cellulase (0.1%, w/v) and Amp, and then grown under shaking conditions (125 rpm) (pre-culture). The pre-culture was further grown for 5 days in total, with a culture medium exchange after the first 48 h. After the pre-culture, cells in each culture were pelleted and resuspended in fresh medium without cellulase (main culture), respectively. The main culture was grown statically for 36 or 72 h to produce pellicles. All culture processes were conducted at 30 °C.

The following three types of pellicle were used in this study: (i) *In vivo* HA/BC nanocomposite pellicles (*in vivo* HA/BC) produced by Gh(HA); (ii) *in situ* HA/BC nanocomposite pellicles (*in situ* HA/BC) secreted from Gh(pTI99) in a mixed culture comprising a normal BC production medium and commercial sodium hyaluronate (0.5%, w/v); and (iii) native BC pellicles (native BC) produced by Gh(pTI99) as a reference.

The pellicles were purified with a combination method of enzymatic treatments using lysozyme and NaOH/sodium dodecyl sulfate (SDS), as previously described (Takahama et al. 2021).

Biodegradation of nanocomposites, HA extraction, and quantitative HA assay

Lyophilized pellicles were immersed in a cellulase mixture (1 mL, cellulase “ONOZUKA” R-10, 0.5% (w/v) in 50 mM sodium acetate buffer). The initial enzyme/pellicle weight ratio was 1:3.5 ± 0.3. The mixtures were incubated in a water bath at 50 °C for 48 h to digest pellicles. The supernatants were separated from the residues by centrifugation (14,000 ·g, 10—15 min). HA in each supernatant was purified by ethanol precipitation, and then quantified using a Hyaluronan Quantification Kit (PG Research Inc., Tokyo, Japan), which determines the HA concentration on the basis of competitive ELISA-like methods using hyaluronan binding protein as the detector. The amount of HA released from each pellicle (μg/g) was calculated by dividing the total HA in the supernatant (μg) by the weight of solubilized (digested by cellulase) pellicles (g). Cellulase treatment did not affect the HA assay (see Figs. S1b and S1c), as confirmed by measuring HA in HA solutions (100 ng/mL) with or without cellulase (Fig. S1b).

The residues separated from supernatants were washed once with 50 mM sodium acetate buffer and once with water, and then freeze-dried. The dry weight of each residue was measured to calculate the rate of solubilization with enzymatic digestion by cellulase. Each residue (approximately 2 mg) was mixed with fine potassium bromide (KBr) powder (200 mg) to prepare KBr pellets. Fourier-transform infrared spectroscopy (FT-IR) were recorded by a FT/IR-6700 spectrophotometer (JASCO Inc., Tokyo, Japan) equipped with a triglycine sulfate detector over the wavenumber range of 4000 to 400 cm^{-1}, using 64 scans with a 2-cm^{-1} resolution. The spectra were normalized using the band at 1060 cm^{-1}, corresponding to C–O stretching (Kondo 1997).

Enzymatic HA extraction was conducted by ionic liquid pretreatment, as follows. Lyophilized pellicles were dissolved (or dispersed) in 60% (w/v) tetrabutylphosphonium hydroxide (TBPH) under shaking at 240 rpm and 30 °C for 72 h, respectively. Cellulose was regenerated from each TBPH solution (or pellicle dispersion in TBPH) by adding 1 M NaCl solution, and HA was precipitated from the supernatant by adding ethanol. The regenerated cellulose and precipitated HA obtained from each pellicle were combined, treated with 1 mL of the cellulase mixture, and then purified by adding trichloroacetic acid and diethyl ether, followed by ethanol precipitation. The amount of HA extracted from each pellicle was measured using the ELISA-like HA assay method.

Confocal laser scanning microscopy (CLSM)

Purified pellicles were fluorescently labelled with Calcofluor White M2R (Sigma-Aldrich) (CW) by immersing pellicles in 10 μg/mL CW solution. After staining, pellicles were washed with DI water, cut into square pieces with sides of approximately 10 mm, and placed in glass dishes for microscopic imaging.

Three-dimensional images of the pellicles were obtained using a confocal laser scanning microscope (TCS SP8, Leica Microsystems, Germany) with 100·/1.4 NA oil immersion objective. The fluorophore was excited by a 405-nm diode laser and fluorescence was detected at 415–470 nm. The voxel size was set as 28 nm · 28 nm · 110 nm based on the ideal Nyquist sampling criterion. 29.06 · 29.06 · 5.07 μm^3 regions were imaged at depths a few micrometers from the surface.

The thicknesses of never-dried pellicles were measured by CLSM before dynamic mechanical analysis (described later). CW-stained pellicle test pieces, which were made from the same culture batch, were observed with a 10· objective, and the thicknesses were calculated at three positions and averaged for each test piece based on distances between the z-positions of the bottom and top surfaces for each pellicle of *in vivo* HA/BC, *in situ* HA/BC, and native BC.

Normal human epidermal keratinocytes grown on the pellicles were observed with the following laser settings for excitation (l_{ex}) and detection (l_{em}): l_{ex} = 486 nm and l_{em} = 498–557 nm for phalloidin (F-actin); l_{ex} = 405 nm and l_{em} = 410–478 nm for Hoechst 33342 (nucleus). The methods for sample staining and image analysis are described later.

Network structure analysis of CLSM images of pellicles

Quantitative analysis of the network structure was performed using open-source program SOAX (Xu et al. 2015) following Mohan's procedure (Mohan et al. 2017). Prior to image analysis, 3D fluorescent images were deconvoluted using commercial deconvolution program Huygens Professional (Scientific Volume Imaging, The Netherlands) with a theoretical point spread function. The deconvoluted images were then preprocessed using a gaussian blur filter and enhanced contrast by ImageJ Fiji (Schindelin et al. 2012), and resized to 256 · 256 pixels for image analysis. 3D reconstructions using SOAX were performed by detecting and tracing the centerlines of the fibrils based on the fluorescent intensity distribution.

Dynamic mechanical analysis (DMA)

Never-dried purified pellicles were cut into dumb-bell-shaped test pieces (ISO 37, type 4) and the thickness value described above was employed. The dynamic viscoelasticity of samples was measured underwater using a DVA-200 instrument (IT Keisoku Co. Ltd., Osaka, Japan) equipped with a temperature control system in stretch deformation mode at a dynamic strain of 0.1% with multiple frequencies (0.1, 1, and 10 Hz). Elastic moduli (storage modulus (*E'*) and loss modulus (*E"*)) of pellicles of *in vivo* HA/BC, *in situ* HA/BC, and native BC were measured at 37 °C and averaged for five individual test pieces. To examine temperature-dependency, elastic moduli were measured with increasing water temperature from 30 to 80 °C at a heating rate of 3 °C. The loss tangent (tand = *E"*/*E'*), as an index of the viscous characteristics, was also obtained.

Human epidermal cell culture on nanocomposite sheets

Aseptically purified pellicles were placed into glass dishes (diameter, 35 mm; IWAKI Co., Ltd. Tokyo Japan) and air-dried at 25 °C on a clean bench to become fixed to the bottom of the dishes. The as-prepared pellicle templates were sterilized under UV light for 1 h, and then soaked in growth medium (HuMedia-KG2, Kurabo Industries Ltd.). Normal human epidermal keratinocytes (NHEK) (Epidercell Human Epidermal Keratinocyte, Kurabo Industries Ltd., 0.8 · 105 cells/mL) were seeded onto all pellicle samples (0.5 · 104 cells/well) simultaneously. The samples were incubated at 37 °C under 5% CO_2 in a humidified chamber for 48 and 96 h, respectively. The growth medium was replaced every 24 h during the culture period.

The pellicles on dishes were washed once with phosphate buffered saline (PBS, pH 7.4), fixed with 3.7% (w/v) paraformaldehyde in PBS (pH 7.0) for 10 min at 25 °C, and permeabilized with 0.5% Triton X-100 in PBS for 5 min at 25 °C. The fixed cells were then incubated with fluorescent phalloidin conjugate (Acti-stain 488 phalloidin, Cytoskeleton Inc. Denver, CO, USA) and nucleic acid staining reagent (Hoechst 33342, Thermo Fisher Scientific Inc., Tokyo, Japan). The stained cells were washed three times with PBS and ProLong Antifade Reagent was added before observations.

The stained samples were observed by CLSM and the images were processed using LAS X software (construction of three-dimensional images) and ImageJ/Fiji software. F-actin images visualized with fluorescent phalloidin were used to estimate cell spreading areas on substrates (Trappmann et al. 2012). Three individual F-actin images (1.16 mm · 1.16 mm) of each group were analyzed using ImageJ/Fiji software for quantification of the cell count (cells/mm^2), total cell area (%), and projected cell area (μm^2) using the following procedures. After the range of pixel values was normalized (contrast stretching with 1% float), the 8-bit images were filtered (smoothing with a median filter) and binarized using a threshold of fixed value. White areas in the binary images were then segmented by applying the watershed algorithm, followed by particle analysis. The selected particles were compared with the original images and then incorrectly segmented areas were removed from the selections prior to calculations. The calculated values were compared statistically between groups using the Tukey–Kramer test (cell count and total cell area) and Steel–Dwass test (projected cell area), with $p < 0.05$ considered statistically significant (*) in both cases.

All statistical analyses were performed using the programs in R software (The R Foundation).

Results And Discussion

Biodegradability, HA extractability, and HA content of HA/BC nanocomposites

The functional mechanism of cellulases and related carbohydrate-degrading enzymes on complex cellulosic biomass suggests that the enzymatic degradation efficiency is highly affected by the natural state of the assembly (Igarashi et al. 2007; Sakuragi et al. 2018). Therefore, it might be helpful to examine the reactivity of nanocomposites toward cellulase to understand their structural features.

Figure 1 shows the results for cellulase degradation of pellicles with or without TBPH (Abe et al. 2012) pretreatment. The degradation rates of the nanocomposites after 48 h of enzymatic hydrolysis (without TBPH pretreatment) varied depending on the group, showing a statistically significant ($p < 0.05$) difference between *in vivo* HA/BC and native BC (Fig. 1a). The lower degradability of *in vivo* HA/BC indicated that HA prevented the cellulase attacking the BC surfaces. FT-IR difference spectra of the residue of *in vivo* HA/BC after cellulase treatment showed two major absorption peaks corresponding to amide groups (1651 cm^{-1} and 1521 cm^{-1}, corresponding to amide I and amide II, respectively; Fig. S1a) (Gilli et al. 1994), indicating that HA remained in the solid even after cellulase treatment.

Figure 1b shows that, while approx. 300 μg of HA was released per 1 g of dried pellicle from *in situ* HA/BC as a reference, *in vivo* HA/BC released only approx. 0.14 μg/g of HA. In contrast, the amount of HA released by *in vivo* HA/BC was substantially higher, by approx. 95 μg/g, under cellulase treatment in combination with TBPH (60% (w/v)) pretreatment, as shown in Fig. 1c. In contrast, the amount of HA released from *in situ* HA/BC remained almost constant, regardless of TBPH pretreatment. Here, the estimated HA contents of the HA/BC nanocomposites were approx. 95 μg/g for *in vivo* HA/BC and approx. 300 μg/g for *in situ* HA/BC.

Although the reaction mechanism of TBPH on native crystalline cellulose (Abe et al. 2012) is not fully understood, these results indicated the difference in HA–BC interaction between *in vivo* and *in situ* HA/BCs, with HA appearing to be more strongly adsorbed on the solid BC surface of *in vivo* HA/BC. The lower HA detection in *in vivo* HA/BC compared with native BC after cellulase treatment without TBPH pretreatment (Fig. 1b) might be attributed to this strong HA adhesion. Another possibility is that HA adsorbed on the solid BC particle was contaminated, which competitively inhibited HA detection in the ELISA-like HA assay system. In either case, HA molecules in *in vivo* HA/BC were found to be strongly associated with BC as a result of *in vivo* fabrication by *G. hansenii*.

Quantitative structural analysis of BC nanofibril network

To quantitatively compare the network structures of the three BC pellicles, 3D image analysis was performed. High-resolution microscopy together with image processing/analysis techniques enables understanding of complex 3D networks of biopolymers, especially in cytoskeletal filaments (Özdemir and Reski 2021). These image analysis methods are also applicable to nanocelluloses that have a similar size scale to cytoskeletal filaments (Mohan et al. 2017). The SOAX program, based on an active contour algorithm, automatically identifies fibrils and junctions from 3D fluorescent microscopic images of filamentous networks (Xu et al. 2015). Using SOAX, all the coordinates of fibrils and junctions are computed and the parameters describing network structure can be obtained. Therefore, SOAX was applicable to quantitative analysis of the network structure of BC pellicles.

Figures 2a–2f show 3D fluorescent images of the BC pellicles (Figs. 2a–2c) and the corresponding SOAX-extracted networks (Figs. 2d–2f). The junction density, which is the number of nanofibril junctions per unit volume, was calculated as shown in Fig. 2g. The junction densities of both *in vivo* and *in situ* HA/BCs were lower than that of native BC with a statistically significant difference.

Pellicles of *in vivo* HA/BC were slightly thicker than those of native BC, whereas those of *in situ* HA/BC were significantly thinner than those of both native BC (by 30%) and *in vivo* HA/BC (by 38%) (Fig. S2). Assuming that the values in Fig. 2g reflected the overall structure of pellicles, the relative whole junction number should be in the order of native BC > *in situ* HA/BC > *in vivo* HA/BC. Notably, further experiments are required to elucidate the detailed structure of these nanocomposites by visualization of HA.

Mechanical characteristics

The hydrated membranous form of BC pellicles is known to be flexible under bending, and strong and stiff under stretch deformation. These characteristics are preferable in biomedical applications, such as wound dressings and implants, where both physical (kinetic) adaptability to the tissues and load-bearing properties are required. However, some reports have indicated that such physical properties can be altered by the intervention of additional polymeric components (Yamanaka et al. 1989; Tajima et al. 1995; Gea et al. 2011), which is of great importance for comparing the mechanical characteristics of nanocomposite pellicles in the present study.

Figure 3 compares the dynamic viscoelasticity data of pellicles acquired at 37 °C underwater with a deformation frequency of 1 Hz. Fig. 3a shows that the storage elastic modulus (*E'*) of *in vivo* HA/BC (approx. 7.5 MPa) was lower than that of native BC (approx. 11.4 MPa). In contrast, both *E'* (approx. 15.6 MPa) and the loss elastic modulus (*E"*, approx. 2.1 MPa) of *in situ* HA/BC were higher compared with those of the other two samples, with statistically significant differences. The thickness of the pellicle test pieces varied depending on the samples (*in vivo* HA/BC > native BC > *in situ* HA/BC (see Fig. S2). The higher *E'* value of *in situ* HA/BC might partly be due to its thinness, which indicates a higher density.

Figure 3. Dynamic viscoelasticity data at 37 °C underwater with a frequency of 1 Hz. (a) Logarithmic plots of storage elastic modulus (*E'*) (●) and loss elastic modulus (*E"*) (△), and their (b) loss tangent (tand). Values were compared statistically using the Tukey–Kramer test, with $p < 0.05$ considered statistically significant (*).

The superior elastic properties of native BC pellicles (as represented by *E'*) were almost maintained in both *in vivo* and *in situ* HA/BCs, with the former tending to be softer and the latter being stiffer. These results indicated that HA–BC interactions between components were different in the two different nanocomposites. The energy dissipation (as represented by tand) of *in vivo* HA/BC was markedly higher than that of *in situ* HA/BC, despite the HA content of the former being indicated as lower than that of the latter (Fig. 1c). This indicated that the nanofibril network structure of *in vivo* HA/BC was more fluid or unstable than that of *in situ* HA/BC, which might be due to the intervention of HA. This indicated that incorporation of other chemical components, such as HA, can negatively affect the physical properties of pellicles (Yamanaka et al. 1989; Gea et al. 2011). Meanwhile, the incorporation of cellulose derivatives (carboxymethyl cellulose and methyl cellulose) via an *in situ* modification method has been reported to more than double the Young's modulus (Tajima et al. 1995). Therefore, the effect of the incorporated polysaccharide component (HA) on the bulk physical properties of the pellicles was considered to be dependent on both the chemical structure and fabrication method. In this regard, our data indicated that HA was likely to interfere with interfibrillar bonding in the *in vivo* method, but reinforce interfibrillar bonding in the *in situ* method. Accordingly, this might explain why *in situ* HA/BC exhibited a markedly higher *E'* value compared with native BC, despite having a significantly lower junction density (Fig. 2g).

Cell culture tests

Human epidermal cell culture experiments were conducted to assess cell–substrate interactions on the surface of nanocomposite pellicles, focusing on cell adhesion, spreading, and cell shape. Cell adhesion to

the material surface is known to be a complex process in which a large number of biological components are involved (Tsimbouri et al. 2014). Among many potential cell-adhesion molecules, clusters of differentiation 44 (CD44) is well-studied for its binding function to glycosaminoglycans, particularly HA, and for its relevant multifaceted physiological functions (Knudson and Peterson 2004; Schmidt and Friedl 2009). CD44 is expressed by almost every vertebrate cell type and is thought to modulate cell mechanics through its connection to the cytoskeleton (Schnauß et al. 2020). In this study, we selected normal human epidermal keratinocyte (NHEK), which has been reported to express CD44 at high levels (*in vivo*) (Carter et al. 1990), and adhesion and subsequent behavior was expected to be altered in response to HA on the substrate surface. As such cell behavior on the surface of a material is often judged and evaluated by visualizing cytoskeletal components, such as filamentous actin (F-actin), and/or by SEM observation (Trappmann et al. 2012; Wang et al. 2012), observation analyses were also adopted in the present study.

Among pellicle samples, *in vivo* HA/BC gave the highest values for both the number of cells attached to surfaces (cell count) (Fig. 4a) and the total area covered with cells (total cell area) (Fig. 4b). NHEK seeded on *in situ* HA/BC sustained both the cell number and total cell area, but the average values were significantly lower than those of *in vivo* HA/BC by over 40% (Figs. 4b, 4c, and S4b). During 48–96 h of culture time, no marked increase in cell count was observed for the nanocomposites, while a decrease was observed for native BC (Fig. 4a). Meanwhile, the total cell areas of *in vivo* and *in situ* HA/BCs increased, indicating that cell spreading occurred on these HA/BC nanocomposite surfaces during this period, as also suggested by the individual cell area values (projected cell area) (Figs. S4a and S4b). In contrast, both the cell count and total cell area of native BC decreased (Figs. 4a and 4b), suggesting relatively poor affinity of its surface for NHEK.

The cell shapes varied depending on the sample. Three-dimensional images constructed from sequence CLSM images showed that the cells attached to *in vivo* HA/BC had irregular shapes (Fig. 4c). Furthermore, as indicated by the white arrowhead in Fig. 4c, colony formation (three or more juxtaposed keratinocytes in contact; Zarkoob et al. 2015) of such irregular-shaped cells was observed only for *in vivo* HA/BC. In contrast, the cells on *in situ* HA/BC showed a more rounded shape, similar to that of native BC. Furthermore, F-actin stained with fluorescent phalloidin showed a more fibrous appearance for *in vivo* HA/BC compared with *in situ* HA/BC and native BC. This indicated a difference in the cytoskeleton physical state between these samples. The difference in cell morphology was confirmed by FE-SEM. Fig. S4c shows the typical flattened cell attached to *in vivo* HA/BC and the spherical cell on native BC as a control.

The cell culture test conducted in the present study clearly showed that the surface of *in vivo* HA/BC was superior to both *in situ* HA/BC and native BC for keratinocyte attachment. HA molecular chains on the *in vivo* HA/BC surface might be immobilized more rigidly than those on *in situ* HA/BC, which was attributed to the substrate provided being suitable for the adhesion of NHEK molecules.

Among many adhesion molecules intrinsic to vertebrate cell systems, integrins and CD44 have been well-studied for their high-affinity binding to both proteins in the extracellular matrix and glycosaminoglycans, such as HA (Schmidt and Friedl 2009). Therefore, both integrins and CD44 might be involved in our experimental results.

Integrins are high-affinity substrates known to cluster to adhesion sites to form complex structures (such as through focal adhesion), which interlink cytoskeletons with the substrate surface (Tsimbouri et al. 2014). Such adhesion structures enable cells to maintain their shape and modulate their behavior in response to substrate stiffness and/or external force (Tsimbouri et al. 2014). As shown in Fig. 4, in contrast to the negative behavior of native BC, both *in situ* and *in vivo* HA/BC substrates showed a greater affinity for such binding. Despite the HA content being indicated as lower than that of *in situ* HA/BC (Fig. 1c), *in vivo* HA/BC showed a higher binding affinity. Furthermore, the more irregular shape and fibrillated appearance of F-actin indicated the formation of a more stable (mature) adhesion structure on *in vivo* HA/BC. In other words, local adhesion sites on *in vivo* HA/BC seemed stiffer than those on *in situ* HA/BC. In future, a more detailed investigation is required.

Conclusions

The current study has investigated the biological and physical characteristics of an *in-vivo*-fabricated HA/BC nanocomposite, in comparison with those of native BC and conventional *in situ* HA/BC. The HA content of *in vivo* HA/BC was estimated to be approx. 95 μg/g, which was one-third that of *in situ* HA/BC. However, HA incorporated into *in vivo* HA/BC was more strongly adsorbed to the solid BC surface, which appeared to significantly affect the biodegradation, mechanical, and cell-adhesive properties. The results clearly showed distinct differences in such material properties caused by the two different methods, namely, *in vivo* and *in situ* fabrication. The enhanced cell–material interactions show that *in vivo* HA/BC has great potential to expand the biomedical use of BC-based materials.

Declarations

Funding

Not applicable

Conflicts of interest/Competing interests

Not applicable.

Availability of data and material

Not applicable.

Code availability

Not applicable.

Author Contributions

Ryo Takahama performed all experiments, except for network structure analysis of pellicles, and prepared the paper; Honami Kato performed human epidermal cell culture examination and provided assistance for HA extraction and quantitative HA assay; Go Takayama performed network structure analysis of pellicles and prepared relevant parts of the paper; Kenji Tajima planned the experiments for biodegradation of nanocomposites, HA extraction, and quantitative HA assay, and assisted with preparing the paper; *Tetsuo Kondo (corresponding author) researched and planned the entire study and prepared the paper. The manuscript was written with contributions from all authors. All authors have approved the final version of the manuscript.

Ethics approval

This study does not include human participants or animal studies.

Consent to participate

All authors (Ryo Takahama, Honami Kato, Go Takayama, Kenji Tajima and Tetsuo Kondo) have approved the manuscript and agreed with submission to Cellulose. The authors have no conflicts of interest to declare.

Consent for publication

We confirm that this manuscript has not been published elsewhere, and is not under consideration in whole or in part by another journal. All authors have agreed with this submission for publication in Cellulose.

References

1. Abe M, Fukaya Y, Ohno H (2012) Fast and facile dissolution of cellulose with tetrabutylphosphonium hydroxide containing 40 wt% water. Chem Commun 48:1808–1810. https://doi.org/10.1039/c2cc16203b
2. Bäckdahl H, Esguerra M, Delbro D, Risberg B, Gatenholm P (2008) Engineering microporosity in bacterial cellulose scaffolds. J Tissue Eng Regen Med 2:320–330. https://doi.org/10.1002/term.97
3. Berti F V., Rambo CR, Dias PF, Porto LM (2013) Nanofiber density determines endothelial cell behavior on hydrogel matrix. Mater Sci Eng C 33:4684–4691. https://doi.org/10.1016/j.msec.2013.07.029
4. Capela D, Barloy-Hubler F, Gouzy J, Bothe G, Ampe F, Batut J, Boistard P, Becker A, Boutry M, Cadieu E, Dréano S, Gloux S, Godrie T, Goffeau A, Kahn D, Kiss E, Lelaure V, Masuy D, Pohl T, Portetelle D, Pühler A, Purnelle B, Ramsperger U, Renard C, Thébault P, Vandenbol M, Weidner S, and Galibert F (2001)

Analysis of the chromosome sequence of the legume symbiont Sinorhizobium meliloti strain 1021. Proc Natl Acad Sci U S A 98:9877–9882. https://doi.org/10.1073/pnas.161294398

5. Carter WG, Wayner EA, Bouchard TS, Kaur P (1990) The role of integrins alpha 2 beta 1 and alpha 3 beta 1 in cell-cell and cell-substrate adhesion of human epidermal cells. J Cell Biol 110:1387–1404. https://doi.org/10.1083/JCB.110.4.1387
6. Fang J, Kawano S, Tajima K, Kondo T (2015) In vivo curdlan/cellulose bionanocomposite synthesis by genetically modified *Gluconacetobacter xylinus*, Biomacromolecules 16: 3154-3160. https://doi.org/10.1021/acs.biomac.5b01075
7. Galibert F, Finan TM, Long SR, Puhler A, Abola P, Ampe F, Barloy-Hubler F, Barnett MJ, Becker A, Boistard P, Bothe G, Boutry M, Bowser L, Buhrmester J, Cadieu E, Capela D, Chain P, Cowie A, Davis RW, Dreano S, Federspiel NA, Fisher RF, Gloux S, Godrie T, Goffeau A, Golding B, Gouzy J, Gurjal M, Hernandez-Lucas I, Hong A, Huizar L, Hyman RW, Jones T, Kahn D, Kahn ML, Kalman S, Keating DH, Kiss E, Komp C, Lelaure V, Masuy D, Palm C, Peck MC, Pohl TM, Portetelle D, B Purnelle, Ramsperger U, Surzycki R, Thebault P, Vandenbol M, Vorholter FJ, Weidner S, Wells DH, Wong K, Yeh KC, and Batut J (2001) The composite genome of the legume symbiont Sinorhizobium meliloti. Science (80-) 293:668–672. https://doi.org/10.1126/science.1060966
8. Gea S, Reynolds CT, Roohpour N, Wirjosentono B, Soykeabkaew N, Bilotti E, Peijs T (2011) Investigation into the structural, morphological, mechanical and thermal behaviour of bacterial cellulose after a two-step purification process. Bioresour Technol 102:9105–9110. https://doi.org/10.1016/J.BIORTECH.2011.04.077
9. Gilli R, Kacuráková M, Mathlouthi M, Navarini L, Paoletti S (1994) FTIR studies of sodium hyaluronate and its oligomers in the amorphous solid phase and in aqueous solution. Carbohydr Res 263:315–326. https://doi.org/10.1016/0008-6215(94)00147-2
10. Gorgieva S (2020) Bacterial Cellulose as a Versatile Platform for Research and Development of Biomedical Materials. Processes 8:624. https://doi.org/10.3390/PR8050624
11. Grobelski B, Wach RA, Adamus A, Olejnik AK, Kowalska-Ludwicka K, Kolodziejczyk M, Bielecki S, Rosiak JM, and Pasieka Z (2014) Biocompatibility of Modified Bionanocellulose and Porous Poly(ϵ-caprolactone) Biomaterials. Int J Polym Mater Polym Biomater 63:518–526. https://doi.org/10.1080/00914037.2013.854223
12. Hall PE, Anderson SM, Johnston DM, Cannon RE (1992) Transformation of Acetobacter xylinum with plasmid DNA by electroporation. Plasmid 28:194–200. https://doi.org/10.1016/0147-619X(92)90051-B
13. Helenius G, Bäckdahl H, Bodin A, Nannmark U, Gatenholm P, Risberg B (2006) In vivo biocompatibility of bacterial cellulose. J Biomed Mater Res - Part A 76:431–438. https://doi.org/10.1002/jbm.a.30570
14. Hutmacher DW, Woodfield TBF, Dalton PD (2014) Scaffold Design and Fabrication. In: Blitterswijk C Van, Boer J De (eds) Tissue Engineering: Second Edition, 2nd edn. Elsevier Science & Technology, pp 311–346

15. Igarashi K, Wada M, Samejima M (2007) Activation of crystalline cellulose to cellulose III(I) results in efficient hydrolysis by cellobiohydrolase. FEBS J 274:1785–1792. https://doi.org/10.1111/j.1742-4658.2007.05727.x
16. Klemm D, Cranston ED, Fischer D, Gama M, Kedzior SA, Kralisch D, Kramer F, Kondo T, Lindström T, Nietzsche S, Petzold-Welcke K, Rauchfuß F (2018) Nanocellulose as a natural source for groundbreaking applications in materials science: Today's state. Mater. Today 21:720–748. https:// 10.1016/j.mattod.2018.02.001
17. Knudson W, Peterson RS (2004) The Hyaluronan Receptor: CD44. In: Garg HG, Hales CA (eds) Chemistry and Biology of Hyaluronan, 1st edn. Elsevier Ltd, pp 83–123
18. Kondo T (1997) The assignment of IR absorption bands due to free hydroxyl groups in cellulose. Cellulose 4:281–292. https://doi.org/10.1023/A:1018448109214
19. Ludwicka K, Jedrzejczak-Krzepkowska M, Kubiak K, Kolodziejczyk M, Pankiewicz T, and Bielecki S (2016) Medical and Cosmetic Applications of Bacterial NanoCellulose. In: Gama M, Dourado F, Bielecki S (eds) Bacterial Nanocellulose: From Biotechnology to Bio-Economy. Elsevier Inc., pp 145–165
20. M. Iguchi;, S. Yamanaka;, A. Budhiono; (2000) Bacterial cellulose - a masterpiece of nature's arts. J Mater Sci 35:261–270. https://doi.org/10.1023/A:1004775229149
21. Mohan S, Jose J, Kuijk A, Veen SJ, Blaaderen A, Velikov KP (2017) Revealing and Quantifying the Three-Dimensional Nano- and Microscale Structures in Self-Assembled Cellulose Microfibrils in Dispersions. ACS Omega 2:5019–5024. https://doi.org/10.1021/acsomega.7b00536
22. Nishi Y, Uryu M, Yamanaka S, Watanabe K, Kitamura N, Iguchi M, and Mitsuhashi S (1990) The structure and mechanical properties of sheets prepared from bacterial cellulose - Part 2 Improvement of the mechanical properties of sheets and their applicability to diaphragms of electroacoustic transducers. J Mater Sci 25:2997–3001. https://doi.org/10.1007/BF00584917
23. Özdemir B, Reski R (2021) Automated and semi-automated enhancement, segmentation and tracing of cytoskeletal networks in microscopic images: A review. Comput Struct Biotechnol J 19:2106–2120. https://doi.org/10.1016/j.csbj.2021.04.019
24. Sakuragi K, Igarashi K, Samejima M (2018) Application of ammonia pretreatment to enable enzymatic hydrolysis of hardwood biomass. Polym Degrad Stab 148:19–25. https://doi.org/10.1016/j.polymdegradstab.2017.12.008
25. Sämfors S, Karlsson K, Sundberg J, Markstedt K, and Gatenholm P (2019) Biofabrication of bacterial nanocellulose scaffolds with complex vascular structure. Biofabrication 11:045010. https://doi.org/10.1088/1758-5090/AB2B4F
26. Schindelin J, Arganda-Carreras I, Frise E, Kaynig V, Longair M, Pietzsch T, Preibisch S, Rueden C, Saalfeld S, Schmid B, Tinevez JY, White DJ, Hartenstein V, Eliceiri K, Tomancak P and Cardona A (2012) Fiji: An open-source platform for biological-image analysis. Nat Methods 9:676–682. https://doi.org/10.1038/nmeth.2019

27. Schmidt S, Friedl P (2009) Interstitial cell migration: integrin-dependent and alternative adhesion mechanisms. Cell Tissue Res 339:83–92. https://doi.org/10.1007/S00441-009-0892-9
28. Schnauß J, Schmidt BUS, Brazel CB, Dogan S, Losert W, Anderegg U, and Käs JA (2020) Influence of hyaluronic acid binding on the actin cortex measured by optical forces. J Biophotonics 13:e201960215. https://doi.org/10.1002/JBIO.201960215
29. Sunagawa N, Tajima K, Hosoda M, Kawano S, Kose R, Satoh Y, Yao M, Dairi T (2012) Cellulose production by Enterobacter sp. CJF-002 and identification of genes for cellulose biosynthesis. Cellulose 19: 1989-2001. https://doi.org/10.1007/s10570-012-9777-2
30. Tajima K, Fujisawa M, Takai M, Hayashi J (1995) Synthesis of Bacterial Cellulose Composite by Acetobacter xylinum I. Its mechanical strength and biodegradability. J Wood Sci 41:749–757.
31. Tajima K, Yao M (2021) Cellulose-synthesizing machinery in bacteria. Cellulose 7:. https://doi.org/10.1007/s10570-021-04225-7
32. Takahama R, Kato H, Tajima K, Tagawa S, and Kondo T (2021) Biofabrication of a Hyaluronan/Bacterial Cellulose Composite Nanofibril by Secretion from Engineered Gluconacetobacter. Biomacromolecules acs.biomac.1c00987. https://doi.org/10.1021/ACS.BIOMAC.1C00987
33. Trappmann B, Gautrot JE, Connelly JT, Strange DGT, Li Y, Oyen ML, Stuart MC, Boehm H, Li B, Vogel V, Spatz JP, Watt FM, and Huck W (2012) Extracellular-matrix tethering regulates stem-cell fate. Nat Mater 11:642–649. https://doi.org/10.1038/nmat3339
34. Tsimbouri PM, Mcnamara LE, Alakpa E V, Dalby MJ, and Turner LA (2014) Cell – Material Interactions. In: Blitterswijk C Van, Boer J De (eds) Tissue Engineering: Second Edition, 2nd edn. Elsevier Science & Technology, pp 217–251
35. Wang Y, Wang G, Luo X, Qiu J, and Tang C (2012) Substrate stiffness regulates the proliferation, migration, and differentiation of epidermal cells. Burns 38:414–420. https://doi.org/10.1016/j.burns.2011.09.002
36. Watanabe K, Eto Y, Takano S, Nakamori S, Shibai H, and Yamanaka S (1993) A new bacterial cellulose substrate for mammalian cell culture - A new bacterial cellulose substrate. Cytotechnology 13:107–114. https://doi.org/10.1007/BF00749937
37. Xu T, Vavylonis D, Tsai FC, Koenderink GH, Nie W, Yusuf E, Lee IJ, Wu JQ, and Huang X (2015) SOAX: A software for quantification of 3D biopolymer networks. Sci Rep 5:. https://doi.org/10.1038/srep09081
38. Yamanaka S, Watanabe K, Kitamura N, Iguchi M, Mitsuhashi S, Nishi Y, and Uryu M (1989) The structure and mechanical properties of sheets prepared from bacterial cellulose. J Mater Sci 24:3141–3145. https://doi.org/10.1007/BF01139032
39. Zarkoob H, Bodduluri S, Ponnaluri S V, Selby JC, and Sander EA (2015) Substrate Stiffness Affects Human Keratinocyte Colony Formation. Cell Mol Bioeng 8:32–50. https://doi.org/10.1007/s12195-015-0377-8

Figures

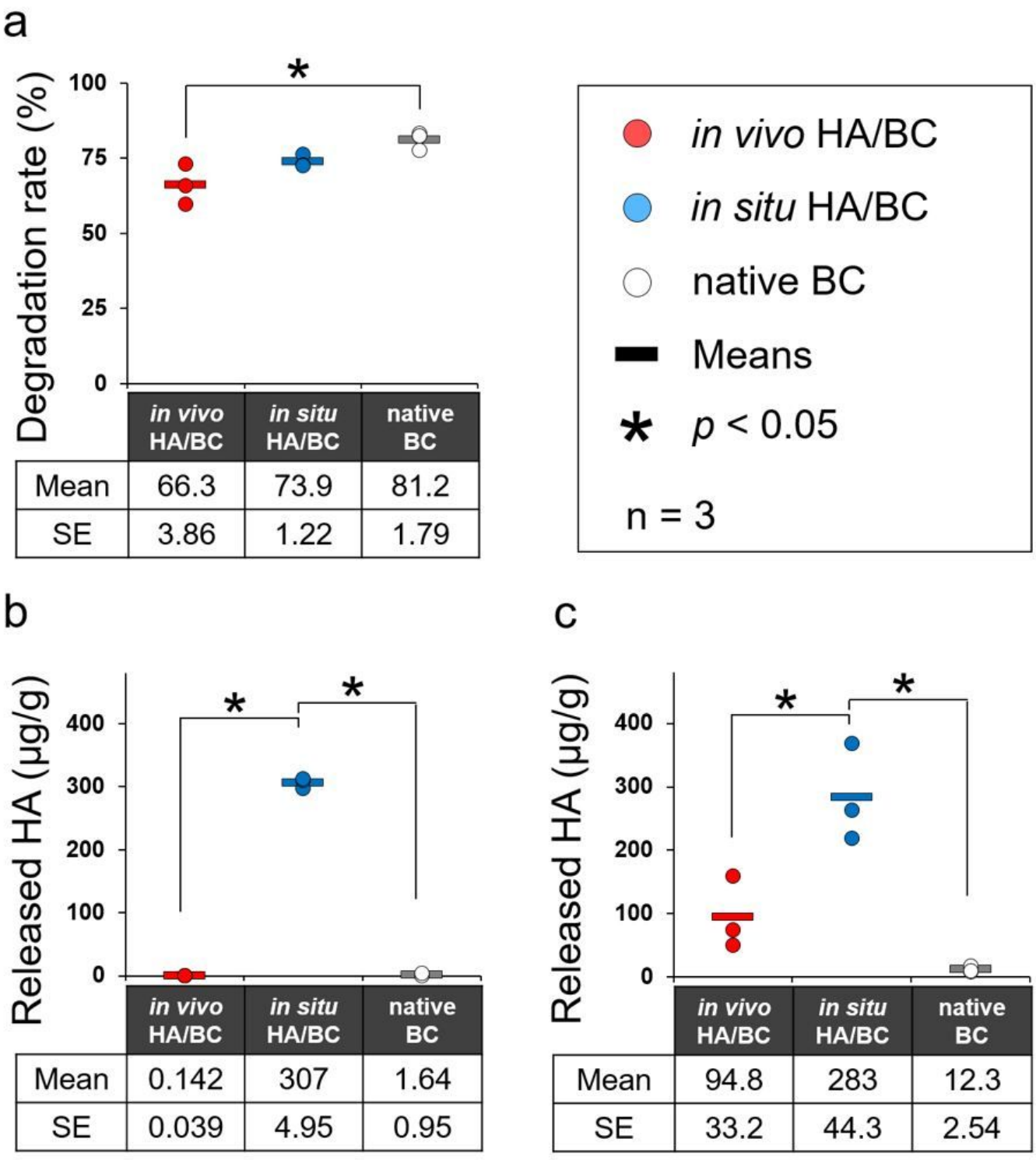

	in vivo HA/BC	in situ HA/BC	native BC
Mean	66.3	73.9	81.2
SE	3.86	1.22	1.79

	in vivo HA/BC	in situ HA/BC	native BC
Mean	0.142	307	1.64
SE	0.039	4.95	0.95

	in vivo HA/BC	in situ HA/BC	native BC
Mean	94.8	283	12.3
SE	33.2	44.3	2.54

Figure 1

(a) Enzymatic degradation rates of pellicles. (b) Amount of HA released from pellicles after cellulase treatment, measured by ELISA-like HA assay. (c) Amount of HA released from pellicles after pretreatment

with 60% (w/v) TBPH–water solution. Values were compared statistically between groups using the Tukey–Kramer test, with $p < 0.05$ considered statistically significant (*).

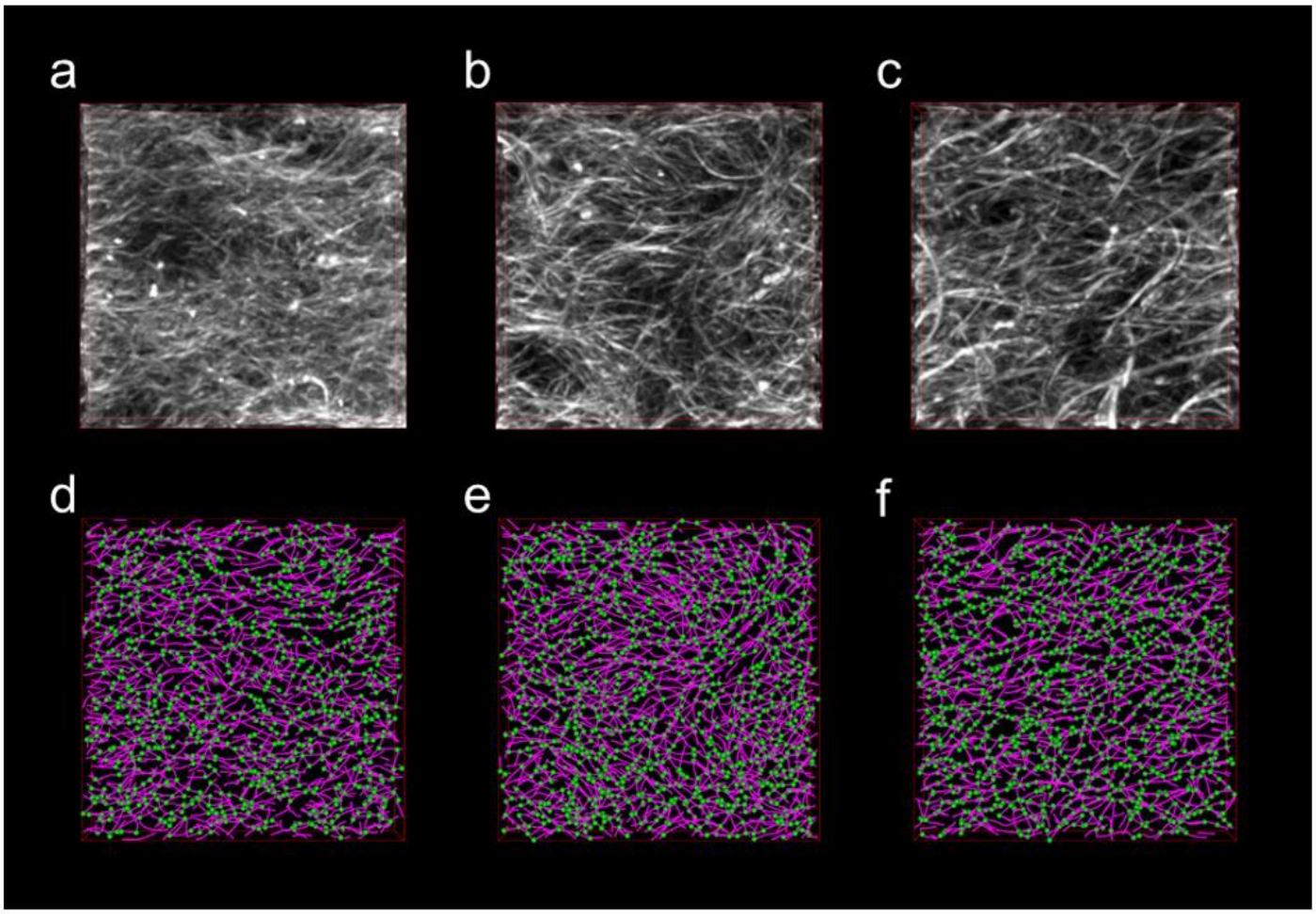

g

	Junction density (/mm^3)	
in vivo HA/BC	$(2.28 \pm 0.06) \times 10^8$	*
in situ HA/BC	$(2.53 \pm 0.26) \times 10^8$	*
native BC	$(3.25 \pm 0.06) \times 10^8$	

Figure 2

3D fluorescent images (upper) and 3D reconstructed images (lower) of (a, d) in vivo HA/BC, (b, e) in situ HA/BC, and (c, f) native BC pellicles. Magenta lines and green dots indicate fibrils and junctions, respectively. Image size was 29.06 x 29.06 x 5.07 μm3. (g) Junction density as mean value for each sample calculated based on analysis. Values were compared statistically between groups using the Tukey–Kramer test, with $p < 0.05$ considered statistically significant (*).

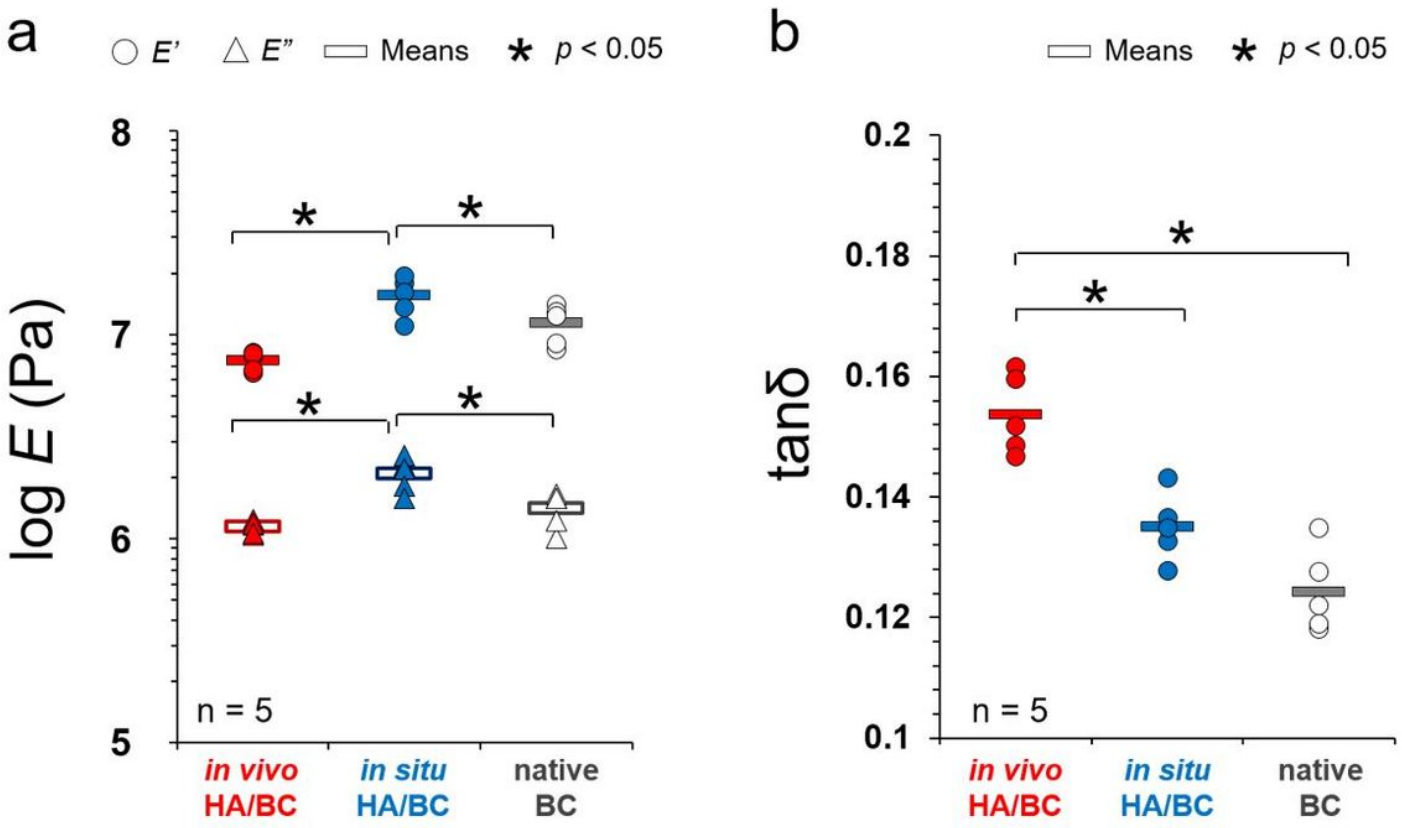

Figure 3

Dynamic viscoelasticity data at 37 °C underwater with a frequency of 1 Hz. (a) Logarithmic plots of storage elastic modulus (E') (●) and loss elastic modulus (E") (△), and their (b) loss tangent (tanδ). Values were compared statistically using the Tukey–Kramer test, with $p < 0.05$ considered statistically significant (*).

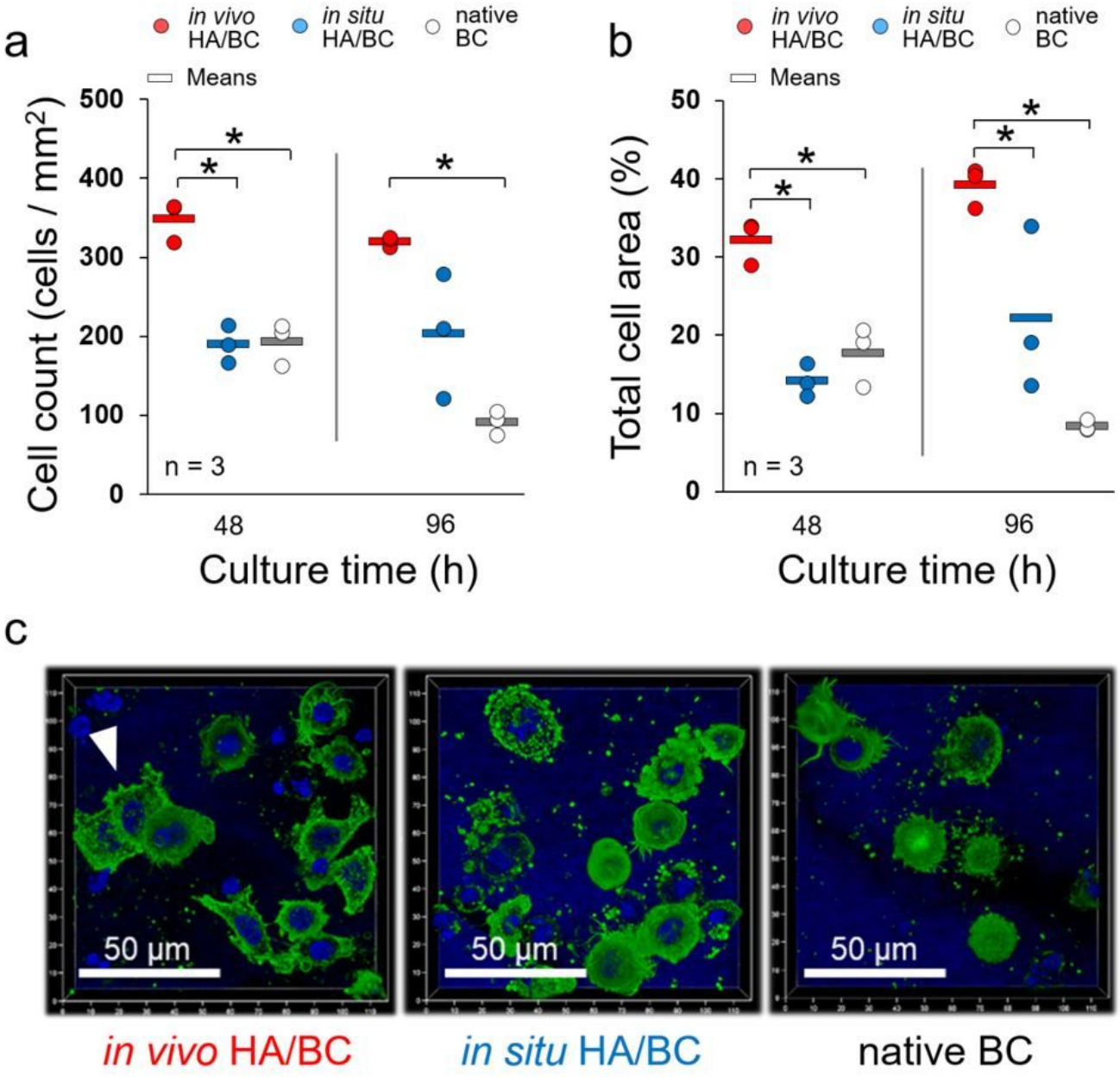

Figure 4

Cell culture test on nanocomposite pellicles. (a) Numbers of cells on pellicles, counted with ImageJ software. (b) Total cell area on pellicles calculated with ImageJ software. (c) Three-dimensional images constructed from sequence CLSM images. Cytoskeletal F-actin and nucleus were stained with fluorescent phalloidin conjugate (green) and Hoechst 33342 (blue). Calculated values were compared statistically using the Tukey–Kramer test, with $p < 0.05$ considered statistically significant (*).

Supplementary Files

This is a list of supplementary files associated with this preprint. Click to download.

- GraphicalAbstract.tif
- TakahamaetalSI20211125.docx